ADVANCED OPTICAL MATERIALS
www.advopticalmat.de

Circularly Polarized Emission from Mixture of Vacuum-Evaporated Mesogenic Luminophores

Chang-Jae Yu, Dong-Myung Lee, Jin-Kyung Han, You-Jin Lee, Sa-Wook Kim, E-Joon Choi, and Jae-Hoon Kim**

Direct circular polarized (CP) emission from a twisted mesogenic luminophore is one of the promising approaches for generating high degree of CP light since device parameters governing the degree of CP emission are easily controlled. Most high CP emissions have been performed by solution process since a twisted structure of mesogenic luminophore is easily achieved. However, since solution process has been impeded by the limitation of low resolution and efficiency, vacuum evaporation has been commonly used in display industries to obtain high performance and resolution. Here, high CP electroluminescence (CPEL) with a dissymmetric factor of 0.914 is demonstrated through the sequential vacuum evaporation of two mesogenic luminophores and chiral agent. The sequentially evaporated luminophores and chiral agent are converted into a mixture by thermal annealing, and the luminophore mixture constructs a twisted structure and generates resultantly high CPEL. The electroluminescence device fabricated with the mixture exhibits three times higher luminance and two times higher efficiency than the devices with each single luminophore. Further, the dissymmetric factors according to the device parameters based on the Stokes parameter analysis are theoretically investigated. It is anticipated that the approach paves the way toward improving CPEL performance.

1. Introduction

Direct emission of circularly polarized (CP) light from luminophores has been interestingly studied for improving devices performances in optical data storages, optical quantum information, and light source applications, such as displays and chirality sensors.[1–7] Especially, in the display industries using organic light-emitting diodes using a circular polarizer to eliminate ambient light reflected from metal cathode, the direct CP emission with the same handedness of the circular polarizer paves the way toward improving the light-extracting efficiency.[8,9] The CP light is generated by molecular chirality of an emitting layer (EML)[10–13] or by macroscopic helical conformation of birefringent luminophores.[9,14–17] In the twisted structure of the mesogenic luminophores prepared by solution processes by containing a chiral agent[9,17] or by inducing different interfacial treatments,[18,19] especially, degree of the CP light is easily controlled by the twist angle and thus high CP light is generated. However, solution process to obtain high degree of CP electroluminescence (CPEL) has been impeded by the limitation of low pixel resolution in the display industry, where vacuum-evaporating process is commonly used to obtain high performance and resolution.

Herein, we demonstrate high CPEL while improving luminance intensity and the efficiency through the sequential vacuum evaporation of two mesogenic compounds and a chiral agent. High CPEL dissymmetric factor of 0.914 was achieved in twisted structure by annealing the mesogenic compounds and chiral dopant thermally after vacuum evaporating them. In the blended mesogenic luminophores by thermal annealing, the electroluminescent (EL) luminance was three times brighter than in each single luminophore, and the efficiency was twice higher. The twist structure of the vacuum-evaporated luminophores by the chiral dopant was investigated with the transmittance and polarization analysis based on a simple light-propagating model in the continuously twisted birefringent medium. In addition, the dissymmetric factors in both photoluminescent (PL) and EL processes were theoretically evaluated according to the twist angle of the blended mesogenic luminophores and the emission zone was estimated by using the Stokes parameter analysis for the EL dissymmetric factor. Further, we theoretically predict the dissymmetric factor in both PL and EL processes for various device parameters and provide design conditions of devices for better performance. In our approach, the optimized devices in various applications are also easily fabricated since the blending ratio and twist angle are controlled by the evaporating thickness.

C.-J. Yu, D.-M. Lee, J.-K. Han, Y.-J. Lee, J.-H. Kim
Department of Electronic Engineering
Hanyang University
Seoul 04763, Republic of Korea
E-mail: cjyu@hanyang.ac.kr; jhoon@hanyang.ac.kr
S.-W. Kim, E.-J. Choi
Department of Polymer Science and Engineering
Kumoh National Institute of Technology
Gumi 39177, Korea
The ORCID identification number(s) for the author(s) of this article can be found under https://doi.org/10.1002/adom.202101674.

DOI: 10.1002/adom.202101674

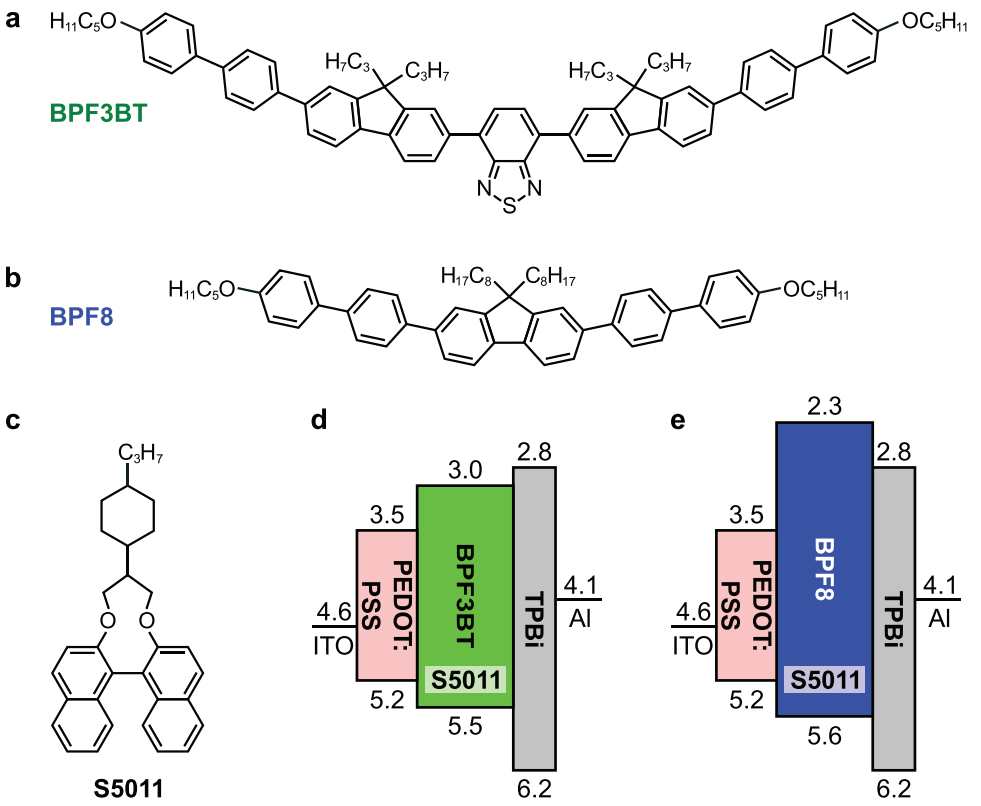

Figure 1. Chemical structures and energy levels. The chemical structures of two luminophores of a) **BPF3BT** and b) **BPF8**, and c) a chiral dopant of **S5011**. The energy level diagrams of the EL devices with d) **BPF3BT** and e) **BPF8**.

2. Results and Discussion

Two mesogenic luminophores of 4,7-bis[7-[4′-(*n*-pentyloxy)-1,1′-biphenyl-4-yl]-9,9-bis(*n*-propyl)fluoren-2-yl]-2,1,3-benzothiadiazole (**BPF3BT**) and 2,7-bis[4′-(*n*-pentyloxy)-1,1′-biphenyl-4-yl]-9,9-bis(*n*-octyl)fluorene (**BPF8**)[20] and a chiral dopant of **S5011** are used as a EML. We fabricated the photoluminescence (PL) devices with two mesogenic luminophores the chiral dopant by thermal evaporation on the rubbed poly(3,4-ethylenedioxythiophene) polystyrene sulfonate (**PEDOT:PSS**) layer to investigate the characteristics of the CP emission. The chemical structures of both mesogenic luminophores and the chiral dopant are shown in **Figure 1**a–c and the energy diagrams in Figure 1d,e. To generate the twisted structure of the mesogenic luminophores, the chiral dopant of **S5011** with high helical twisting power (HTP) was thermally evaporated on each mesogenic luminophore and the PL devices were thermally annealed at each mesogenic temperature (see the Experimental Section; and Figure S1a,b, Supporting Information). In the mesogenic conjugate polymer prepared by solution-process, the chiral dopant generated the twisted configuration and thus the high CP light emitted.[9,21]

In the evaporated **BPF3BT** sample (see the device architecture in **Figure 2**a and the absorption/emission spectra in Figure S1c, Supporting Information), the PL spectra under left-handed circular polarizer (LHCP) and right-handed circular polarizer (RHCP) were identical at both its mesogenic temperature (260 °C) and room temperature (see Figure 2b,c). In the polarizing microscopic textures, good dark state was also observed when the rubbing direction of the **PEDOT:PSS** was parallel to one of crossed polarizers (see insets in Figure 2b,c). This means that the **BPF3BT** film with **S5011** exhibits uniaxial property and its optic axis is parallel to the rubbing direction since the chirality of the dopant appears only in a limited temperature range.[22] In addition, the transmittance of the **BPF3BT+S5011** film, measured by rotating the film under crossed polarizers (see the measurement setup in Figure S2a, Supporting Information), confirmed that the **BPF3BT** molecules was unidirectionally aligned along the rubbing direction (see the Experimental Section; and Figure S2b, Supporting Information). It should be noted that the CP emission does not generated in the unidirectionally aligned structure since the polarization direction of the emitted light coincides with the optic axis of the birefringent layers and thus there is no change in the polarization state even if it passes through the birefringent layers.

In the evaporated **BPF8** sample (see the device architecture in Figure 2d and the absorption/emission spectra in Figure S1d, Supporting Information), the PL spectra under LHCP and RHCP were obviously distinguished at its mesogenic temperature (140 °C) (see Figure 2e). In the polarizing microscopic textures, no dark state was observed at any directions (see insets in Figure 2e) and thus the **BPF8** film with **S5011** would be twisted differing from the **BPF3BT+S5011** film. At room temperature, however, the PL spectra under LHCP and RHCP were identical, and good dark state was also observed similar to the **BPF3BT+S5011** film, probably due to the large elasticity (see Figure 2f). The transmittance of the **BPF8+S5011**

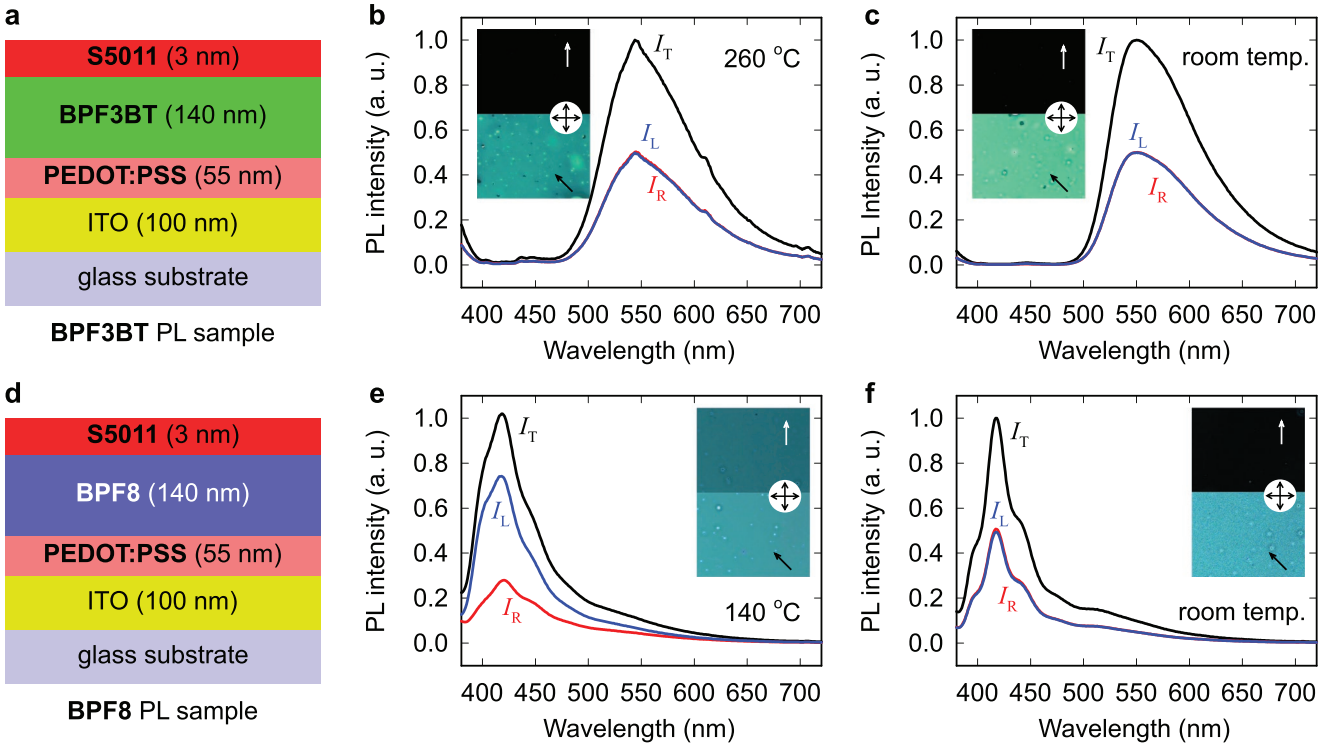

Figure 2. The CPPL spectra and textures of **BPF3BT** and **BPF8** samples. Schematic diagrams a,d) and the PL intensities and the polarizing microscopic textures of the **BPF3BT** and **BPF8** samples at each temperature of its mesogenic phase b,e) and at room temperature after cooling down rapidly c,f). Arrows in textures represent the rubbing directions of the **PEDOT:PSS** and two-way arrows depict the directions of the crossed polarizers in microscope.

film confirmed that the **BPF8** molecules were unidirectionally aligned along the rubbing direction (see Figure S2c, Supporting Information).

In the liquid crystal (LC) applications, mixtures blended with several LC single compounds were generally used to optimize the material properties and improve the device performance.[23] Similarly, we sequentially evaporated **BPF8**, **BPF3BT**, and **S5011** due to the different evaporation conditions (see the device architecture in **Figure 3**a). In the stacked **BPF8**/**BPF3BT** sample, the PL spectra under LHCP and RHCP were obviously distinguished at both its mesogenic temperature (140 °C) and room temperature (see Figure 3b,c). Note that the emission spectrum of **BPF8** is overlapped with the absorption spectrum of **BPF3BT**, and thus the emission spectrum of the stacked **BPF8**/**BPF3BT** film is similar with that of the single **BPF3BT** film (see Figure S1c,d, Supporting Information). In addition, in the mixture of **BPF8** and **BPF3BT** with 1:1 mixing ratio, the mesogenic temperature is reduced to 104 °C, which is lower than that of the single compounds (see Figure S3, Supporting Information). This means that the mixture blended with two mesogenic luminophores exhibits material properties as a third substance not a simple host-guest system. In addition, various mixing ratio is easily controlled by each evaporating thickness.

The degree of circular polarizations is typically defined by the dissymmetry *g* factor as follows

$$g = 2\frac{I_L - I_R}{I_L + I_R} \quad (1)$$

where I_L and I_R denote the intensities of LHCP and RHCP light, respectively. The g_{PL} factors at the mesogenic temperature and room temperature in the PL process were evaluated to be 0.64 and 0.53 at 546 nm, respectively (see the Experimental Section for measurement details; and Figure 3b,c). To investigate the origin of the CP emission with such high *g* factor, first, the polarizing microscopic textures were observed at two sample directions rotating by 0° and 45° with respect to polarizer (see insets in Figure 3b,c), and no dark state was observed at any directions from the transmittance measured by rotating the film under crossed polarizers (see Figure S4a, Supporting Information). Using the simple model of the continuously twisted mesogenic medium,[9,18] the measured transmittance was fitted to Equation S1 (Supporting Information) and the fitted twist angle was evaluated to be 83.5° (see the Experimental Section for evaluation details; and solid line in Figure S4a, Supporting Information). To confirm that the stacked **BPF8**/**BPF3BT** film formed the twisted structure, we also measured the Stokes parameters passing through the **BPF8**/**BPF3BT** film at 546 nm and compared the calculated Stokes parameters according to the total twist angle based on the model of the continuously twisted mesogenic medium. The twist angle was determined to be 81.2°, which is coincident with the fitted twist angle to Equation S1 (Supporting Information) (see the Experimental Section for evaluation details; and Figure S4b, Supporting Information). We also investigated the PL device fabricated by different evaporation sequence of **BPF3BT**, **BPF8**, and **S5011** (see the Supporting Information for investigation details). The similar CPPL results were observed as shown in

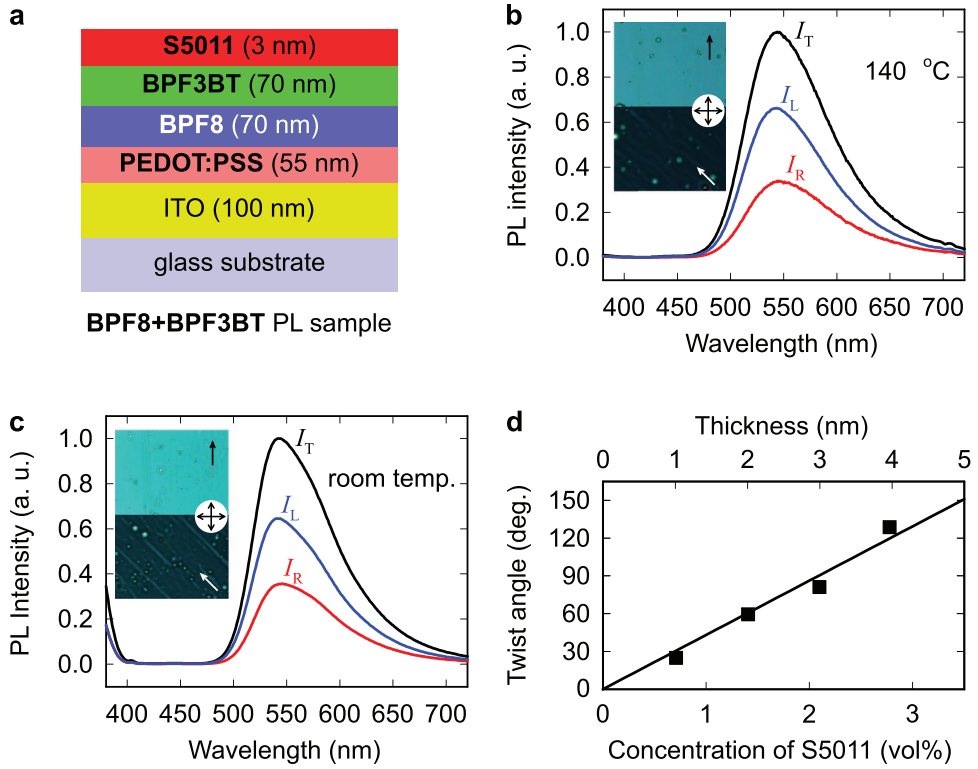

Figure 3. The CPPL spectra and textures of the stacked **BPF8**/**BPF3BT** sample. a) Schematic diagram and the PL intensities and the polarizing microscopic textures of the stacked **BPF8**/**BPF3BT** sample with 2.1 vol% of **S5011** b) at temperature of its mesogenic phase and c) at room temperature after cooling down rapidly. d) The measured twist angle (symbols) of the stacked **BPF8**/**BPF3BT** was linearly proportional to thickness (volume concentration) of **S5011**. The slope of the straight line was fitted to be 43.1 deg vol%$^{-1}$. Arrows in textures represent the rubbing directions of the **PEDOT:PSS** and two-way arrows depict the directions of the crossed polarizers in microscope.

Figure S5a (Supporting Information) but longer annealing time was required experimentally than the device prepared by the sequentially evaporated **BPF8**, **BPF3BT**, and **S5011**. Since longer annealing time gave rise to degradation of the device efficiency in the EL devices as shown in Figure S5b (Supporting Information), we mainly focused the stacked **BPF8**/**BPF3BT** film.

Next, we varied an evaporating thickness of **S5011** on the stacked **BPF8**/**BPF3BT**, corresponding to the concentration of the chiral dopant, and measured the twist angle (see Figure 3d). As you know, the twist angle of the nematic LC molecules is linearly proportional to concentration of the chiral dopant for a given thickness.[9,24] The slope of the straight line was fitted to be a 43.1 deg vol%$^{-1}$, which corresponded to be 84.0 μm^{-1} of the HTP, defined as the inverse of the product of the concentration of the chiral dopant and the resulting pitch of the twisted structure.[24] The chiral dopant **S5011** or **R5011** (isomer of **S5011**) has been widely used to generate a large twist angle in nematic LCs with a short pitch due to the large HTP of about 100 μm^{-1} and also recently used to construct the twisted structure of the mesogenic polymer.[9,18,25] As you know, the HTP is strongly dependent on the host molecules (molecular sterics and weight), and generally decreases with increasing molecular weight and vice versa. The evaluated HTP of 84.0 μm^{-1} is within a reasonable range considering that the HTP is about 100 μm^{-1} for typical nematic LCs with lighter molecular weight than the mixture of **BPF8** and **BPF3BT**, and about 10 μm^{-1} for mesogenic polymers.

From the above results, the thermally evaporated **BPF8**/**BPF3BT**+**S5011** films construct the continuously twisted configuration of the mesogenic thin sublayers after thermal annealing and quenching. Also, we investigated the dissymmetric factors of the evaporated **BPF8**/**BPF3BT**+**S5011** films with different twist angles changing the evaporating thickness of **S5011** to reaffirm the validity of the continuously twisted EML proposed here. We measured the twist angles and the PL *g* factors for the **BPF8**/**BPF3BT** films with different thicknesses of **S5011**. As shown in **Figure 4**a–c, the g_{PL} factors of the **BPF8**/**BPF3BT**+**S5011** films were measured from the PL intensities under LHCP and RHCP at 546 nm using Equation (1) (see the Experimental Section for measurement details).

The continuously twisted structure of the **BPF8**/**BPF3BT**+**S5011** film can be regarded as a helicoidal arrangement of birefringent sublayers since the **BPF8**/**BPF3BT** film exhibits birefringence. Each birefringent sublayer emits the linearly polarized (LP) light after absorbing UV light and the LP light propagates sequentially the twisted sublayers experiencing the phase retardation. For example, the LP light emitted at the sublayer closest to the detector is measured as the LP light since there is no phase retardation. On the other hand, the LP light emitted at the sublayer farthest from the detector experiences the phase retardation through the entire twist sublayers. The phase retardation and the resulting polarization state are directly calculated with sequential product of Müller matrix described with the birefringence and the twist

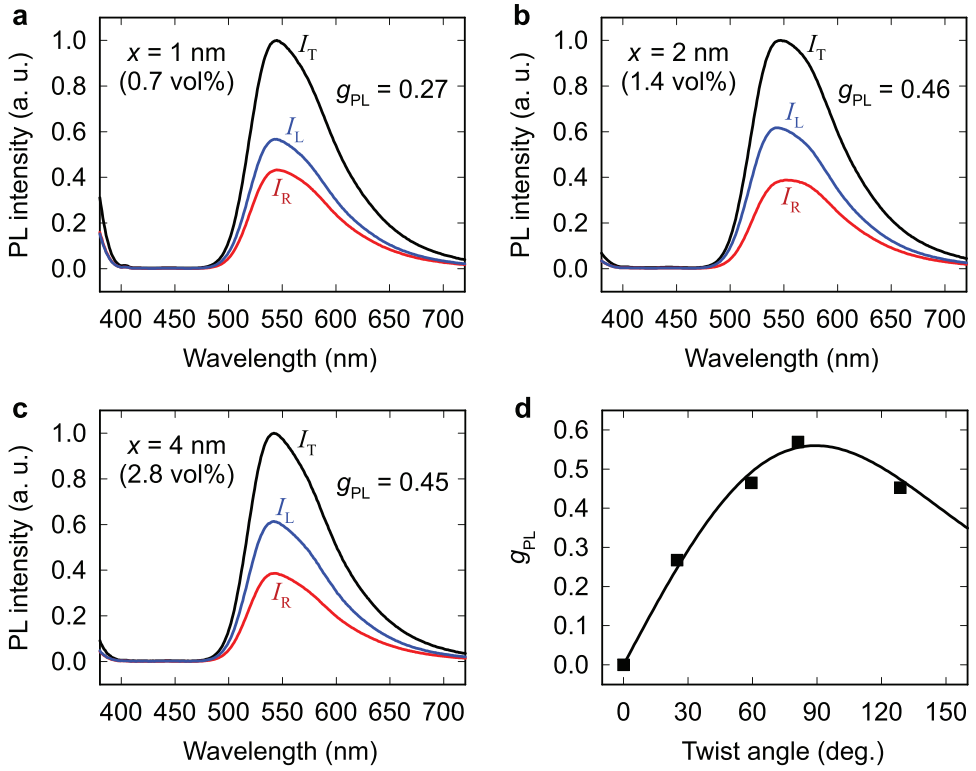

Figure 4. The g_{PL} factors of the PL devices with various concentration (thicknesses) of **S5011**. PL intensities of the **BPF8**/**BPF3BT** samples with a) 0.7 (1 nm), b) 1.4 (2 nm), and c) 2.8 (4 nm) vol% of **S5011** under no circular polarizer (I_T, black line) and under LHCP (I_L, blue line) and RHCP (I_R, red line). The g_{EL} values are determined by the EL intensities at 546 nm using the definition of the dissymmetric *g* factor. d) The g_{EL} factors (symbols) for the EL devices according to the twist angle of the blended **BPF8**/**BPF3BT**+**S5011** layer. The solid line depicts the theoretical calculations based on the Müller matrix analysis for the CPEL mechanism.

angle in each sublayer.[9] Now, to evaluate the theoretical g_{PL} factor in our model, several parameters, such as thickness, twist angle, birefringence, and degree of linear polarization of the EML are mandatorily required (see the Experimental Section for calculation details).[9,18,21] The birefringence of the mesogenic thin sublayer was evaluated from measuring the optical phase retardation according to the sample rotating angle under crossed polarizers[21,26] and determined to be 0.6444 at 543.5 nm (see the Experimental Section for measurement and calculation details and Figure S6, Supporting Information). Since the LP light emitted at each sublayer was not fully polarized in practical experiments, the theoretical g_{PL} factor should be corrected to the degree of linear polarization, which was determined to be 0.8794 at 546 nm (see the Experimental Section for measurement and calculation details; and Figure S7a, Supporting Information). Now, the theoretical g_{PL} factor was directly calculated according to the twist angle using the device parameters such as thickness, twist angle, birefringence, and degree of linear polarization (see the Experimental Section for calculation details). It should be noted that all device parameters were measured and evaluated independently of the measured g_{PL} factor and the theoretical g_{PL} factor was calculated directly without any fitting parameter. The theoretical g_{PL} factor was coincident with the measured g_{PL} factor as shown in Figure 4d, and thus our continuously twisted model was reaffirmed in the system with the thermally evaporated luminophores and chiral dopant.

Similarly, we fabricated the EL devices by deposited with 2,2′,2″-(1,3,5-benzentriyl)-tris(1-phenyl-1-H-benzimidazole (**TPBi**), LiF, and Al on the **BPF8**/**BPF3BT**+**S5011** film as shown in **Figure 5**a. The EL spectra of the **BPF8**/**BPF3BT** film with 3 nm thick **S5011** were measured under LHCP and RHCP at 546 nm as shown in Figure 5b. The other EL devices of the **BPF8**/**BPF3BT** films with different concentrations (thicknesses) of **S5011** were shown in Figure S8 (Supporting Information) and the corresponding the EL *g* factors according to the twist angle were evaluated from EL intensities under LHCP and RHCP at 546 nm (see the Experimental Section for measurement details, and squares in Figure 5c). Note that the twist angle is controlled by the evaporated thickness of **S5011** (concentration of **S5011**). The g_{EL} factor is governed by an essential parameter of emission zone (recombination zone), which affects the optical and electrical properties.[21,27] To calculate the theoretical g_{EL} factor, we also introduce the helicoidal arrangement of birefringent sublayers as mentioned in the PL *g* factor. In the EL device, it must be considered that the LP light emitted at a specific sublayer (emission zone) propagates the twisted birefringent sublayers toward the anode and cathode unlike the PL device. It should be noted that only the light propagating toward the detector is considered in the PL device since there is no cathode acted as a reflector. At first, the light propagating toward the anode experiences the phase retardation through the twisted sublayers from the emitted sublayer to the anode (the detector-side). On the other hand, the light propagating

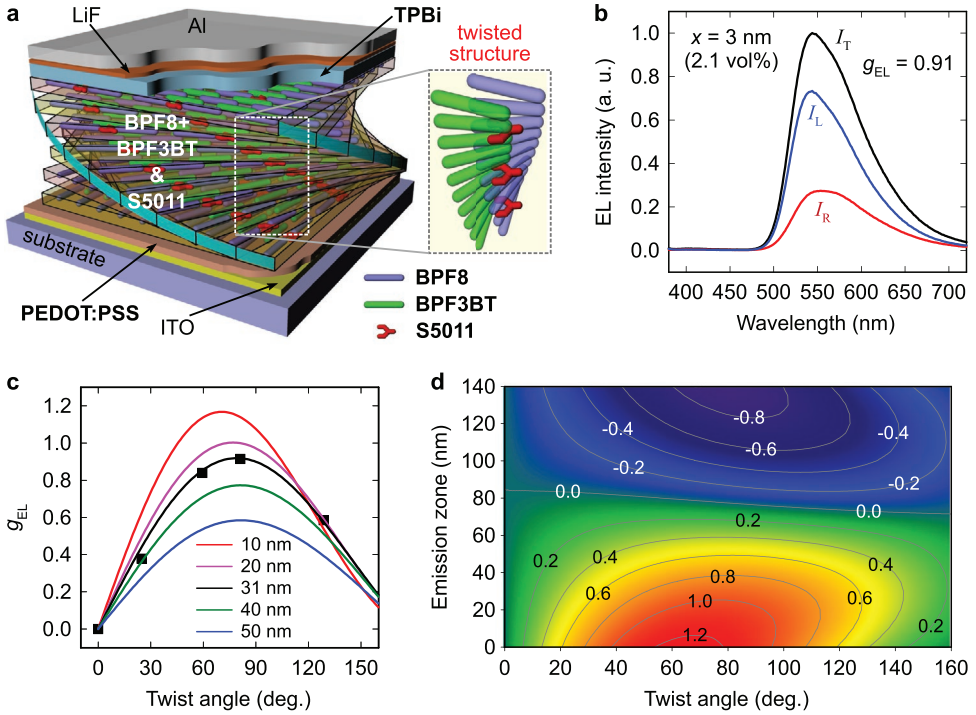

Figure 5. The EL mechanism and the g_{EL} factors of the EL devices. a) Schematic diagram of the EL mechanism with the blended **BPF8**/**BPF3BT** layers. b) EL intensities of the **BPF8**/**BPF3BT** sample with 2.1 vol% of **S5011** under no circular polarizer (I_T, black line) and under LHCP (I_L, blue line) and RHCP (I_R, red line). c) The g_{EL} factors the EL devices according to the twist angle of the blended **BPF8**/**BPF3BT**+**S5011** layer. Squares represent the measured data and solid lines depict the theoretical calculations at different emission zones (a distance from the **TPBi** layer) based on the Müller matrix analysis for the CPEL mechanism. d) The simulated g_{EL} factor of the 142 nm thick sample according to the twist angle and the emission zone is shown on the contour map.

toward the cathode experiences the phase retardation through the twisted sublayers from the emitted sublayer to the cathode and experiences reversely through the entire twisted sublayers after reflection from the cathode. Note that the propagating probabilities toward both electrodes are the same as each other and the cathode is assumed to reflect completely.

The measured polarization state and the corresponding g_{EL} factor for a given emission zone are also directly calculated with sequential product of Müller matrix as mentioned in the PL g factor.[9,18,21] From the measured g_{EL} factors according to the twist angle, the emission zone can be estimated by calculating the theoretical g_{EL} factor since all device parameters except for the emission zone were already obtained independently of the measured g_{EL} factor. The thickness and the twist angle of the **BPF8**/**BPF3BT**+**S5011** films were already determined and the birefringence (0.6444 at 543.5 nm) used the result measured in the PL process. The degree of linear polarization in the EL device was determined to be 0.9038 at 546 nm by using a ratio of linear polarization of the **BPF8**/**BPF3BT** film without **S5011** (Experimental Section for measurement and calculation details; and Figure S7b, Supporting Information). Varying the specific sublayer emitting the LP light (emitting zone), the g_{EL} factor was calculated as a function of the twist angle at the averaged thickness (142 nm) of the **BPF8**/**BPF3BT**+**S5011** films. Finally, the emission zone of the distance from the isotropic **TPBi** layer (the cathode-side) was determined to be 31 nm by applying the least-square-error to the measured g_{EL} factor (Figure 5c). In the calculation for the emission zone of 31 nm, the maximum g_{EL} factor of 0.92 was observed at the twist angle of 79° (the optimal twist angle). As the emission zone moves toward the cathode, the g_{EL} factor gradually increases but the optimal twist angle with the maximum g_{EL} factor slightly decreases.

3. Conclusion

The theoretical g_{EL} factor of the 142 nm thick film was also calculated according to the twist angle and the emission zone (Figure 5d). As you expect, the implementation of the birefringent medium is a key parameter in the g_{EL} factor and, in the acute angle range, the g_{EL} factor gradually increases as the emission zone moves to zero (toward the cathode). Interestingly, as the emission zone moves to 140 nm (toward the anode), the sign of the g_{EL} factor is inversed and the absolute value of the g_{EL} factor increases, which means that the CPEL with the reversed handedness can be generated. In the CPEL mechanism mentioned above, if the emission zone is placed near **PEDOT:PSS**, where the negative g_{EL} factor appears in out simulation as shown in Figure 5d, the light propagating toward the anode does not experience the phase retardation and thus the LP state is still maintained. Consequently, the LP light contributes equally to the intensities of the LHCP and RHCP lights. On the other hand, the light propagating toward cathode (reflector) experiences the phase retardation passing

through the twisted structure and reversely experiences after reflection from the cathode. The LP state can change from the LHCP state to the RHCP state as the total phase retardation increases. As the emission zone moves to anode, the total phase retardation experienced by the light propagating toward the cathode increases. As a result, the intensity of RHCP light is greater than that of LHCP light in a certain condition and thus the negative g_{EL} factor appears. The emission zone is governed by the thicknesses of the EML, the **PEDOT:PSS**, and **TPBi** layers.[21]

The luminance intensities of the devices fabricated with each synthesized luminophore (**BPF3BT** and **BPF8**) without chiral dopant and the blended luminophores with the 3 nm thick **S5011** (**BPF8**/**BPF3BT**+**S5011**) were measured to be 442, 91, and 1335 cd m^{-2}, respectively (Figure S9, Supporting Information). Also, the maximum efficiencies of the **BPF3BT**, **BPF8**, and blended **BPF8**/**BPF3BT** devices were measured to be 1.60, 0.91, and 2.86 cd A^{-1}, respectively. In the blended **BPF8**/**BPF3BT** device, EL emission was three times brighter than in **BPF3BT** device and the efficiency was about twice higher due to the spectrum overlapping between the emission of **BPF8** and the absorption of **BPF3BT**.

In this study, we have demonstrated that thermally evaporated mesogenic luminophores and chiral dopant constructs the twisted structure after thermal annealing and quenching and the high degree of dissymmetric factor was obtained, while improving the luminance intensity and the efficiency. The importance of this result is highlighted by blending the mesogenic luminophores by stacking them sequentially with thermal evaporation to achieve material properties required for fabricating the high CP device. Furthermore, the theoretical g_{PL} and g_{EL} factors were estimated according to the twist angle and the emission zone based on the proposed Müller matrix analysis. Such blending approach will be of great interest in the current display and lighting industry using vacuum evaporation, and also open new ways for novel applications in high performed biosensors and displays. Future blended EMLs with further optimization will have higher dissymmetric factor and enable better efficiency by controlling a blending ratio and synthesizing new luminophores.

4. Experimental Section

Materials: Two mesogenic luminophores of 4,7-bis[7-[4′-(*n*-pentyloxy)-1,1′-biphenyl-4-yl]-9,9-bis(*n*-propyl)fluoren-2-yl]-2,1,3-benzothiadiazole (**BPF3BT**) and 2,7-bis[4′-(*n*-pentyloxy)-1,1′-biphenyl-4-yl]-9,9-bis(*n*-octyl)fluorene (**BPF8**) were synthesized,[20] and the left-handed chiral dopant of **S5011** was received from Merck. The chemical structures of all materials used in EML layer are shown in Figure 1a–c. Poly(3,4-ethylenedioxythiophene) polystyrene sulfonate (**PEDOT:PSS**) and 2,2′,2″-(1,3,5-benzentriyl)-tris(1-phenyl-1-H-benzimidazole (**TPBi**) were commercially acquired from Lumtec and used as a hole injection layer and an electron transport layer, respectively. The energy levels of the **BPF3BT** and **BPF8** devices are summarized in Figure 1d,e. The mesogenic temperatures of **BPF3BT** and **BPF8** were measured at 254 and 123 °C during heating, respectively (see Figure S1a,b, Supporting Information). In the **BPF3BT**, two absorption peaks were observed at 340 and 425 nm, and the emission peak appeared at 557 nm. In the **BPF8**, the absorption peak was observed at 345 nm and the emission peak appeared at 413 nm (see Figure S1c,d, Supporting Information). The phase transition temperature was determined by differential scanning calorimeter (DSC 200 F3, NETZSCH) performed in a nitrogen atmosphere with heating and cooling rates of 10 °C min^{-1}.

Device Fabrication: Prepatterned indium-tin-oxide (ITO) substrate (about 20 Ω sq^{-1}) with thickness of 100 nm was rinsed by ultrasonication with deionized water and mucasol (alkali detergent) for 60 min. After treating the ITO substrate with oxygen plasma, the **PEDOT:PSS** with a thickness of 55 nm was spin-coated at 3000 rpm for 20 s and 1000 rpm for 10 s and baked at 100 °C for 10 min. To promote unidirectional alignment of the mesogenic luminophores, the baked **PEDOT:PSS** was rubbed by a rubbing machine (RMS-50-M, Nam Il Optical Instruments).[8] **BPF3BT**, **BPF8**, and **S5011** were deposited by thermal evaporation (6×10^{-6} torr) and annealed for 60 s at each mesogenic temperature (260 °C for **BPF3BT** and 140 °C for **BPF8**). After rapid quenching the deposited film with liquid nitrogen to maintain the alignment as in its mesogenic phase, the PL devices were characterized, and **TPBi** (20 nm), LiF (1 nm), and Al (70 nm) were deposited by thermal evaporation (6×10^{-6} torr) for characterizing the EL devices. The thermal annealing and the quenching were performed in glove box with a nitrogen atmosphere.

Alignment Characteristics: The alignment textures were observed by a polarizing microscope (E600W POL, Nikon) with image-grabbing system (SDC-450, Samsung) under crossed polarizers. To investigate the uniaxiality of the anisotropic EML, transmittance was measured under crossed polarizers according to a rotating angle of the sample with respect to the polarizer (see Figure S2a, Supporting Information). In a unidirectionally aligned mesogen, the normalized transmittance represents the minimum intensity (zero intensity) when the optic axis of the uniaxial medium is parallel to either of two crossed polarizers. The maximum transmittance occurs when the optic axis of the uniaxial medium rotates by 45° with respect to either of two crossed polarizers (see Figure S2b,c, Supporting Information).[28] In a twisted medium, the minimum transmittance does not reach zero in any rotating angle of the sample with respect to the polarizer (see Figure S4a, Supporting Information). Detail relationship between transmittance and the sample-rotating angle under crossed polarizers was expressed in the Supporting Information.

Twist Angle Measurement: For determining the twist angle of the EML, the Stokes parameters, passing through the EML of an incident probing light with linear polarization, were measured and compared to the theoretically evaluated Stokes parameters passing through the continuously twisted mesogenic layers of the LP incident light according to the total twist angle for a given thickness (see Figure S4b, Supporting Information).[20,29] Also, the twist angle above was reaffirmed by comparing the fitted twist angle to Equation (S1) (Supporting Information).

Birefringence Measurement: The optical phase modulation method with a PEM (PEM-100, Hinds) and a lock-in amplifier (SR830, Stanford Research System) was used to measure the optical retardation of the stacked **BPF8**/**BPF3BT** film without a chiral dopant.[20,26] Experimental setup consists of the PEM and the sample mounted on a rotary stage under crossed polarizers (see Figure S6a, Supporting Information). The phase retardation $\Gamma(\theta)$ was measured with the photodetector and lock-in amplifier as a function of the sample-rotating angle θ with the relationship as follows, (see the Supporting Information for calculation detail)

$$\Gamma(\theta) = \tan^{-1}\left[\frac{2\sin(\Gamma_0)\cos(2\theta)}{1-\cos(4\theta)+\{1+\cos(4\theta)\}\cos(\Gamma_0)}\right] \quad (2)$$

After fitting the measured phase retardation to Equation (2), finally the birefringence of the EML is calculated using the fitting parameter Γ_0 considering the thickness of the EML and wavelength of the probing light (543.5 nm).

Degree of Linear Polarization: The PL/EL intensities of the staked **BPF8**/**BPF3BT** film whose rubbing direction is parallel and perpendicular to linear polarizer are measured without chiral dopant. The degree of linear polarization was evaluated from the ratio of the intensity difference between the parallel and perpendicular

contributions to the sum of the two intensities at 546 nm[18,19] (see Figure S7, Supporting Information).

Dissymmetric g Factor Measurement: The CPPL of the single **BPF3BT**, and the CPPL and CPEL of the stacked **BPF8**/**BPF3BT** were measured with spectroradiometer (SR-UL 1R, TOPCON) under the LHCP and RHCP consisting of a linear polarizer and a quarter-wave-plate as 546 nm. Both PL and EL *g* factors were calculated from the PL and EL intensity at 546 nm by using the definition of the *g* factor. The CPEL of the single **BPF8** was measured using the circular polarizer consisting of a linear polarizer and a quarter-wave-plate as 415 nm and the corresponding *g* factor was evaluated at 415 nm.

Calculation of the Dissymmetric g Factor in PL Device: For calculating the PL *g* factor, it was assumed that the EML is uniformly twisted and divided to *N* sublayers with uniaxial property as assumed in determination of the twist angle.[18,19] In the PL process, at all sublayers, the UV light is absorbed and the visible light is emitted with linear polarization. The LP light produced at the *i*th sublayer subsequently propagates the twisted sublayers from the *i*th to *N*th sublayers, experiencing the phase retardation. The polarization state passing through the twisted sublayers is expressed as the Stokes parameters $\mathbf{S}(i)$ and directly calculated with sequential product of Müller matrix described with the phase retardation of each sublayer and the rotating angle between adjacent sublayers.[18,19] For simplification, the interlayer effects were neglected, such as absorption, reflection, and scattering during light propagation. It should be noted that the emitting probability at each sublayer is the same in the PL process. In this way, the polarization states for all emitting sublayers are described as the Stokes parameters, and thus the final polarization state of the PL process is expressed by an average of all Stokes parameters of the polarization states emitted at the individual sublayers since the Stokes parameters are represented as some algebra of energy values. By the definitions of the dissymmetric *g* factor and the Stokes parameters, the *g* factor is $-2S_3$. In this model, the emitting polarization state at each sublayer was assumed to generate completely linear polarization. On the other hand, since the degree of the linear polarization was finite in the measurement, the theoretically evaluated *g* factor should be corrected to the degree of linear polarization of the sample (see Figure 6a). The PL *g* factors are directly evaluated without any fitting parameters for various twist angles and compared with the measured *g* factors (see Figure 4d).

Calculation of the Dissymmetric g Factor in PL Device: For calculating the EL *g* factor, it was also assumed that the EML is uniformly twisted and divided to *N* sublayers with uniaxial property as mentioned in the PL process.[18,19] In the EL process, the LP light is emitted only at a certain sublayer (emission/recombination zone) differing from the PL process. The LP light produced at the *i*th sublayer (emission zone) propagates toward both the anode and the cathode passing through the twisted sublayers, experiencing the phase retardation. In the case of the propagating light toward the anode, it subsequently passes through the twisted sublayers from the *i*th to *N*th sublayers. The Stokes parameters expressing its polarization state is calculated with sequential product of Müller matrix described with the phase retardation of each sublayer and the rotating angle between adjacent sublayers.[18,19] In the case of the propagating light toward the cathode, it inversely passes through the twisted sublayers from the *i*th to first sublayers and reflects from the cathode. The reflected light propagates the entire twisted sublayers from the first to *N*th sublayers. Like the PL *g* factor, the interlayer effects during light propagation were neglected. It should be noted that the emitting probabilities toward both electrodes are the same as each other. The final polarization state is expressed by an average of two Stokes parameters for both propagating lights and the dissymmetric *g* factor is calculated to be $-2S_3$. Like the PL *g* factor, the theoretically evaluated *g* factor should be corrected to the degree of linear polarization of the sample (see and Figure 6b). The EL *g* factors for various twist angles are fitted only with the emission zone and compared with the measured *g* factors (see Figure 5c).

Electrical Measurement: The current density–voltage–luminance characteristics of the EL devices were measured at room temperature using a spectroradiometer, a programmable power supply (PPE-3323, GW Instek), and a multimeter (Keithley 2000, Keithley) (see Figure 8).

Supporting Information

Supporting Information is available from the Wiley Online Library or from the author.

Acknowledgements

This work was supported by National Research Foundation (NRF) of Korea (No. NRF-2018R1A2A3075276) and by ITECH R&D program of MOTIE/KEIT (No. 20012560).

Conflict of Interest

The authors declare no conflict of interest.

Data Availability Statement

Research data are not shared.

Keywords

circular polarized electroluminescence, circular polarized photoluminescence, mesogenic luminophores, mesogenic mixture, vacuum evaporation

Received: August 12, 2021
Revised: September 30, 2021
Published online:

[1] C. Wang, H. Fei, Y. Qiu, Y. Yang, Z. Wei, Y. Tian, Y. Chen, Y. Zhao, *Appl. Phys. Lett.* **1999**, *74*, 19.
[2] R. Singh, K. N. Narayanan Unni, A. Solanki, *Opt. Mater.* **2012**, *34*, 716.
[3] C. Wagenknecht, C.-M. Li, A. Reingruber, X.-H. Bao, A. Goebel, Y.-A. Chen, Q. Zhang, K. Chen, J.-W. Pan, *Nat. Photonics* **2010**, *4*, 549.
[4] Y. Yang, R. C. da Costa, M. J. Fuchter, A. J. Campbell, *Nat. Photonics* **2013**, *7*, 634.
[5] J. Han, S. Guo, J. Wang, L. Wei, Y. Zhuang, S. Liu, Q. Zhao, X. Zhang, W. Huang, *Adv. Opt. Mater.* **2017**, *5*, 1700359.
[6] M. Li, Y. F. Wang, D. Zhang, L. Duan, C. F. Chen, *Angew. Chem., Int. Ed.* **2020**, *59*, 3500.
[7] D.-W. Zhang, M. Li, C.-F. Chen, *Chem. Soc. Rev.* **2020**, *49*, 1331.
[8] G. Trapani, R. Pawlak, G. R. Carlson, J. N. Gordon, *US patent 6549335*, **2003**.
[9] D.-M. Lee, J.-W. Song, Y.-J. Lee, C.-J. Yu, J.-H. Kim, *Adv. Mater.* **2017**, *29*, 1700907.
[10] J. R. Brandt, X. Wang, Y. Yang, A. J. Campbell, M. J. Fuchter, *J. Am. Chem. Soc.* **2016**, *138*, 9743.
[11] F. Zinna, M. Pasini, F. Galeotti, C. Botta, L. D. Bari, U. Giovanella, *Adv. Funct. Mater.* **2017**, *27*, 1603719.
[12] G. Albano, L. A. Aronica, A. Minotto, F. Cacialli, L. D. Bari, *Chem. – Eur. J.* **2020**, *26*, 16622.
[13] L. Wan, J. Wade, X. Shi, S. Xu, M. J. Fuchter, A. J. Campbell, *ACS Appl. Mater. Interfaces* **2020**, *12*, 39471.
[14] E. Peeters, M. P. T. Christiaans, R. A. J. Janssen, H. F. M. Schoo, H. P. J. M. Dekkers, E. W. Meijer, *J. Am. Chem. Soc.* **1997**, *119*, 9909.

[15] M. Oda, H.-G. Nothofer, G. Lieser, U. Scherf, C. J. Meskers, D. Neher, *Adv. Mater.* **2000**, *12*, 362.
[16] Y. Yang, R. C. da Costa, D.-M. Smilgies, A. J. Campbell, M. J. Fuchter, *Adv. Mater.* **2013**, *25*, 2624.
[17] S. H. Chen, D. Katsis, A. W. Schmid, J. C. Mastrangelo, T. Tsutsui, T. N. Blanton, *Nature* **1999**, *397*, 506.
[18] K. Baek, D.-M. Lee, Y.-J. Lee, H. Choi, J. Seo, I. Kang, C.-J. Yu, J.-H. Kim, *Light Sci. Appl.* **2019**, *8*, 120.
[19] Y.-K. Seo, Y.-J. Lee, J.-H. Kim, C.-J. Yu, *Adv. Opt. Mater.* **2021**, *9*, 2002020.
[20] S.-W. Kim, D.-M. Lee, J.-H. Kim, E.-J. Choi, C.-J. Yu, *Liq. Cryst.* **2019**, *46*, 1136.
[21] J.-H. Jung, D.-M. Lee, J.-H. Kim, C.-J. Yu, *J. Mater. Chem. C* **2018**, *6*, 726.
[22] D. Yoshizawa, H. Higuchi, Y. Okumurab, H. Kikuchi, *J. Mater. Chem. C* **2019**, *7*, 2225.
[23] M. Schadt, *Annu. Rev. Mater. Sci.* **1997**, *27*, 305.
[24] P. G. de Gennes, J. Prost, *The Physics of Liquid Crystals*, Oxford University Press, New York **1993**.
[25] Y. Shin, Q. Wang, D.-K. Yang, *Soft Matter* **2020**, *16*, 3669.
[26] J.-H. Lee, C.-J. Yu, S.-D. Lee, *Mol. Cryst. Liq. Cryst.* **1998**, *321*, 317.
[27] J. Kim, K.-Y. Kim, J. Kim, *Appl. Opt.* **2018**, *57*, 8394.
[28] P. Yeh, C. Gu, *Optics of Liquid Crystal Displays*, John Wiley & Sons, Hoboken, NJ **2010**.
[29] Y. Zhou, Z. He, S. Sato, *Jpn. J. Appl. Phys.* **1997**, *36*, 2760.